Thermal diffusivity measurement of highly conductive materials using a periodic pulse rear face measurement technique

Emmanuel Ruffio, Jean-Christophe Batsale, Andrzej Kusiak,
Christophe Pradere, Alain Sommier, Jean-Luc Battaglia*
Institute of Mechanical Engineering,
UMR CNRS 5295, University of Bordeaux,
351 cours de la Libération, 33405 Talence Cedex.

Abstract

This paper presents an improvement of the classical flash technique that allows measuring the thermal diffusivity of highly diffusive materials without the need of blackbody coatings. The method consists in heating the front face of the sample using a periodic pulses sequence with suitable period and pulse duration. The rear face temperature is recorded simultaneously. An inverse approach is then used to estimate the thermal diffusivity. The underlying model is completely analytical and includes heat transfer and analog signal processing which has been specifically designed for this experiment. A sensitivity analysis and an experiment optimization are performed. Applied to an uncoated copper sample, this method appears to be reliable even in the case of very low optical emission/absorption. Theoretical expectations have been confirmed from experimental data obtained considering copper. Thermal diffusivity has been estimated with less than 4% on both the standard and absolute deviation.

*Electronic address: jean-luc.battaglia@u-bordeaux.fr

I. INTRODUCTION

Measuring the thermal diffusivity of highly conductive materials remains challenging and large deviations are still observed according to the experimental operating conditions. The classical photothermal methods are based on the thermal response of the sample to a heat pulse, considered as a Dirac function from the mathematical point of view. The temperature increase on the opposite face (rear face) of the excitation is classically measured using an infrared (IR) detector. This so-called flash experimental technique that has been developed first by Parker [1] and that has been improved along time by several contributions [2–5]. An exhaustive list of the developments can be found in [6]. However, highly diffusive sample are generally of metallic nature with very low optical emission/absorption in the visible and infrared wavelengths. Thereby, if no optical transceiver is present on both faces of the sample, the measured signal is very noisy and this leads to poor confidence interval of the identified property. Therefore, classical approach requires depositing thin blackbody coatings on both faces, the one on the front face assuring the maximum energy absorption of the photothermal source whereas the other one on the rear face is assumed to make the emissivity close to one, thus enhancing the signal noise ratio of the IR detector. Those coatings are generally deposited from spray constituted by graphite particles within an epoxy resin [7, 8]. Nevertheless, they have a significant influence on the measured signal according to their thermal properties. This can be easily demonstrated from a model of the one-dimensional heat conduction through a three-layers system [9]. This model can be simulated using the classical quadrupoles method based on integral transform technique [10]. Let us assume for instance a cylindrical sample made of copper (thermal conductivity $k_{Cu} = 400\,\mathrm{W.m^{-1}.K^{-1}}$, specific heat per unit volume $(\rho C_p)_{Cu} = 3.5\,\mathrm{MJ.K^{-1}.m^{-3}}$ and thickness 3 mm) and whose both faces are coated with a graphite-based spray (thermal conductivity $k_d = 1\,\mathrm{W.m^{-1}.K^{-1}}$, specific heat per unit volume $(\rho C_p)_d = 2\,\mathrm{MJ.K^{-1}.m^{-3}}$). The apparent thermal diffusivity of the one-layer sample is reported in Tab.I according to the thickness e_d of the coating. It is clear that a significant difference in the thermal diffusivity of copper ($114.3\,\mathrm{mm^2.s^{-1}}$) occurs when the coating thickness is larger than 10 µm. In addition it is also remarkable that the thermal resistance of one coating is comparable or larger than that of the copper layer ($R_{Cu} = e_{Cu}/k_{Cu} = 7.5 \times 10^{-6}\,\mathrm{K.m^2.W^{-1}}$) when $e_d \geq 10\,\mu\mathrm{m}$. It is thus recommended to control accurately the coating thickness and the contact resistance

e_d µm	0	1	10	20	50
a_{app} mm^2.s^{-1}	114.3	114.3	113.4	109.4	85.4
a_{app} mm^2.s^{-1}[10]	114.3	114.3	113.2	108.9	83.4
$R_d \times 10^{-6}$ K.m^2.W^{-1}	0	1	10	20	50

Table I: Apparent thermal diffusivity a_{app} of a copper sample coated on both faces with graphite-based spray, with respect to the coating thickness e_d. The thermal resistance of the coating $R_d = e_d/k_d$ is also given. First line refers to the diffusivity estimated by an inverse approach (the sample is assumed homogeneous but a 3-layers model is used to simulate experimental data). Second line is the apparent diffusivity given by [10] (Eq.10) . Contact resistance is omitted.

when using a 3-layers model or to find highly diffusive blackbody coatings. Both previous recommendations are not easy to respect given the inherent composition of the spray and the deposition process that is random by nature. In addition, deposition of other coatings using chemical vapor deposition or pressure vapor deposition processes for instance, makes the experiment more complex.

A theoretical solution has been proposed by Vozär et al. [11] that consists in heating the sample using severals pulses in order to increase the amount of energy entering the sample while minimizing temperature gradient. In this paper, a variant of this idea is proposed with the following changes. The photothermal source is now continuously emitting heat pulses at low frequency f_{exc}. As a consequence, the mean temperature of the sample increases slowly. Once the steady periodic regime is reached, the rear face temperature is recorded after every pulses. Thus, N_s pulses lead to N_s columns vectors $T_i(t)$ of temperature values, with $1 \leq i \leq N_s$. Since the temperature evolution is periodic, differences between these N_s vectors are due to the measurement noise only. By computing the average temperature over index i, the resulting vector $\overline{T}(t) = \frac{1}{N_s} \sum_{i=1}^{N_s} T_i(t)$ shows an improved signal noise ratio. Assuming vectors are statistically independent, the noise standard deviation of temperature values $\overline{T}(t)$ is theoretically reduced by $\sqrt{N_s}$ compared to $T_i(t)$. As high as N_s could be ($N_s = 2000$ in this study), it has no effect on the temperature amplitude and low voltage signals have still to be recorded in the case of low optical emission/absorption sample. A specific signal amplifier based on a high-pass filter has been developed.

The experimental setup is presented is section 2. In section 3, the corresponding heat transfer and electrical models are presented and an analytical solution is derived. The photothermal pulse width and the contribution of the filter are considered. A sensitivity analysis is performed in section 4 in order to optimize the experimental operating conditions.

In section 5, the method is applied to a copper sample.

II. EXPERIMENTAL SETUP

The experimental setup is represented schematically in figure 1. It is composed of a Coherent Matrix Q-switch Nd:YAG diode-pumped laser (1064 nm wavelength) delivering pulses in a continuous or burst mode. The pulse width is lower than 40nsec and the maximum pulse frequency is $f_p = 100\,\text{kHz}$. The maximum rms power (10 W) is reached with a pulse frequency of 30 kHz. The laser beam radius is 0.55 mm (< 3 mrad divergence) and it is directed at the front face of the sample. There is no way to produce a pure continuous wave with this laser. Therefore, a finite pulse width excitation is produced by emitting a N_p-pulse train with the laser burst mode. It consists in emitting a quick succession of N_p pulses at frequency f_p. The pulse width being thereby $\Delta t_{burst} = N_p/f_p$. The N_p-pulse train is repeated with frequency f_{exc} using a function generator (Agilent 33320A). This repetition frequency dictates the heat transfer dynamic in the sample. A fast photodiode with 0.5 nsec rise time (Thorlabs DET 10A/M) is used to trigger the acquisition device (a Lecroy Waverunner LT 364 scope). The temperature variations of the rear face are low so that there is a linear relationship between the temperature change and the emitted infrared radiation which is monitored by a HgCdTe photoconductive infrared detector (Judson J15D12) working in the (2-14) µm range with the maximum sensitivity located at 11 µm. The location and solid angle (45°) of the detector are such that the sample is fully contained in the field of view. As a result, the detector output (a variation of electrical resistance R_{det}) is related to the average surface temperature. This configuration allows using non-uniform distribution of the deposited heat flux at the front face as well as wavelength-dependency of optical coefficient. A germanium window (high band-pass optical filter with 1.4 µm cut-off wavelength) is put in front of the detector to reject all laser diffuse reflection that could affect temperature measurements.

As presented in figure 2, the temperature dependent resistance R_{det} of the photoconductive detector is part of a Wheatstone bridge-based circuit leading to a first stage amplification of gain$K_1 = 10$. A 2nd-order high-pass filter of Sallen-Key type is then used in order to remove the time average temperature, i.e. the DC signal, as well as all potential temperature drifts and signal shifts. Thanks to this, the signal variations stay centered on 0 V even with

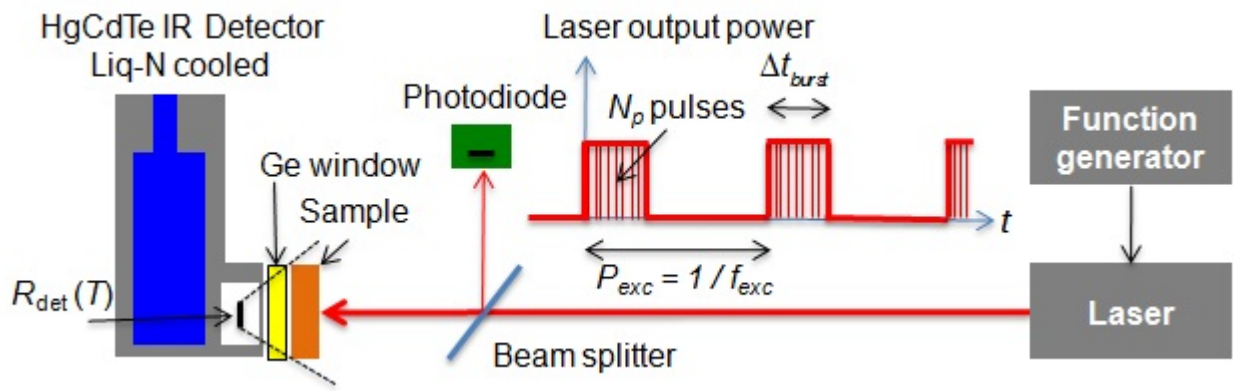

Figure 1: Experimental setup - the photothermal excitation $\phi(r, \theta, t)$ is an N_p-pulse train whose equivalent width is Δt_{burst}, periodically repeated with frequency f_{exc}.

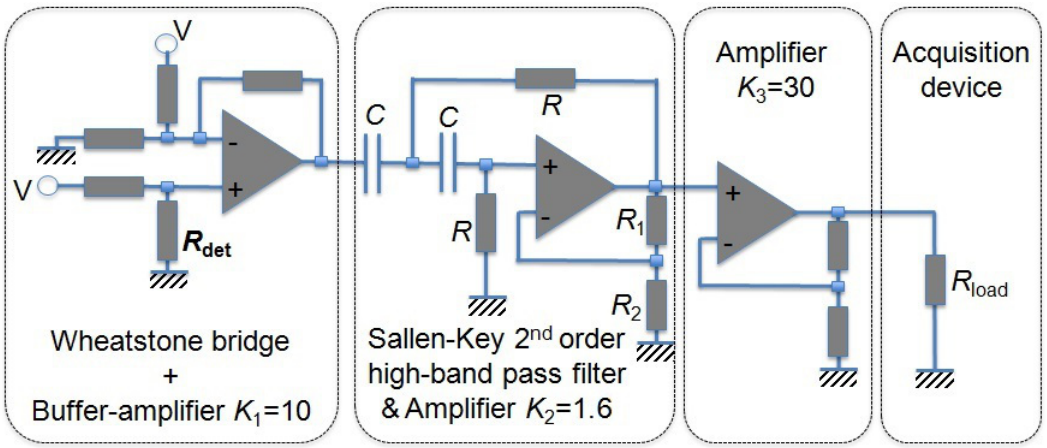

Figure 2: The analog signal processing is a 3-stage amplifier: two amplifiers and one filter.

the lowest scope sensitivity. The gain $K_2 = 1 + R_1/R_2$ is related to the damping factor of the filter. Finally, the signal is amplified by a factor $K_3 = 30$ and recorded using the scope (input impedance $R_{load} = 1\,\mathrm{M}\Omega$, 8 bits vertical resolution, 11 bits resolution for math tools). The signal average is performed over N_s sweeps or sets (up to $N_s = 4000$ with this scope) of N_{data} (up to 50 000) temperature samples.

The overall analog signal processing is described by a 2nd-order transfer function H_f. Some test was carried out with a function generator as input to check the consistency of this model. Results were in good agreement with theoretical expectations [12]. $H_f(j\,\omega)$ is :

$$H_f(j\,\omega) = G\frac{-\omega^2/\omega_c^2}{1 + j\,2\,m\,\omega/\omega_c - \omega^2/\omega_c^2}\,,\; j^2 = -1 \tag{1}$$

With f be the signal frequency under consideration and $\omega = 2\,\pi\,f$ the corresponding

angular frequency. G is the gain. $\omega_c = 2\,\pi\,f_c$ with f_c is the high-pass cut-off frequency. m is the damping factor. The high pass filter is built with potentiometers allowing f_c to vary from 0.1 to 30 Hz. Based on 2, it comes: $\omega_c = 1/RC$ and $m = \frac{1}{2}(3 - K_2)$. Components were chosen in such a way as to get $f_c \approx 0.8\,\text{Hz}$ and $m \in [0.5 - 0.7]$ range. Using a square wave generator as input signal and an inverse approach, it was found $f_c = 0.85 \pm 0.09\,\text{Hz}$ and $m = 0.7 \pm 0.07$. There is no use to estimate precisely the gain G since relation Eq.1 not only includes the signal processing but to optical part as well (emissivity of the sample, solid angle, efficiency and bias current of the detector...).

III. MATHEMATICAL MODEL

Thermal diffusivity and conductivity of the material are denoted a and k respectively. The sample is assumed opaque within the visible and infrared wavelength range. Temperature variations are small enough so that the thermophysical properties are considered constant during the experiment. Heat losses at the front, rear and lateral faces are introduced using heat transfer coefficients, denoted respectively h_h, h_r and h_{lat}. Assuming the sample is a cylinder with radius R and height L, the relative temperature field $T(r,\theta,z,t)$ in a cylindrical coordinate system is given by:

$$\frac{1}{a}\frac{\partial T}{\partial t} = \frac{1}{r}\frac{\partial}{\partial r}\left(r\frac{\partial T}{\partial t}\right) + \frac{1}{r^2}\frac{\partial^2 T}{\partial \theta^2} + \frac{\partial^2 T}{\partial z^2},\ 0 < r < R, \theta, 0 \leq \theta \leq 2\pi,\ 0 < z < e,\ t > 0 \qquad (2)$$

with the associated boundary equations:

$$-k\frac{\partial T(r,\theta,z,t)}{\partial z} = -h_f\,T(r,\theta,z,t) + \phi(r,\theta,t)\,,\ z = 0 \qquad (3)$$

$$-k\frac{\partial T(r,\theta,z,t)}{\partial z} = h_r\,T(r,\theta,z,t)\,,\ z = L \qquad (4)$$

$$-k\frac{\partial T(r,\theta,z,t)}{\partial r} = h_{lat}\,T(r,\theta,z,t)\,,\ r = R \qquad (5)$$

and initial condition:

$$T(r,\theta,z,t) = 0,\ t = 0 \tag{6}$$

The heat flux density is assumed to be a separable function of space and time, i.e. : $\phi(r,\theta,t) = Q\, g(r,\theta)\ f(t)$ with Q the amount of energy absorbed by the sample per pulse. Considering a P_{exc}-periodic emission of single pulse (dirac function), $g(r,\theta)$ and $f(t)$ have the following properties:

$$\int_{r,\theta} g(r,\theta)\, r\, dr\, d\theta = 1 \qquad and \qquad f(t) = \sum_{i=0}^{\infty} \delta(t - i\, P_{exc}) \Rightarrow \int_{t=0}^{P_{exc}} f(t)\, dt = 1 \tag{7}$$

The incoming heat flux density $\phi(r,\theta,t)$ can be splitted in two parts $\phi = E[\phi] + (\phi - E[\phi])$ with $E[\bullet]$ the time-average operator. The system response can be splitted accordingly. It can be expressed as the sum of a "steady" (at least for large time) temperature field $T_c(r,\theta,z,t)$ corresponding to the time-averaged thermal excitation $\phi_c(r,\theta,t) = E[\phi] = Q\, f_{exc}\, g(r,\theta)\ u(t)$ with $u(t)$ the Heaviside function, and a periodic one $T_p(r,\theta,z,t)$ corresponding to the remaining heat flux $\phi_p(r,\theta,t) = Q\, g(r,\theta)\ (-f_{exc} + \sum_{i=0}^{\infty} \delta(t - i\, P_{exc}))\ u(t)$. As long as temperature variations are small and the sample is highly conductive, heat losses can be neglected to solve T_p. Therefore, considering the average surface temperature $\overline{T_p}(z,t) = 1/S \int_{r,\theta} T_p(r,\theta,z,t)\, r\, dr\, d\theta$ with $S = \pi R^2$, previous equations lead to a 1d-heat transfer conduction problem :

$$\frac{\partial \overline{T_p}(z,t)}{\partial t} = a \frac{\partial^2 \overline{T_p}(z,t)}{\partial z^2},\ 0 < z < L,\ t > 0 \tag{8}$$

with the associated boundary equations:

$$-k \frac{\partial \overline{T_p}(z,t)}{\partial z} = \overline{\phi_p}(t)\,,\ z = 0 \tag{9}$$

$$-k \frac{\partial \overline{T_p}(z,t)}{\partial z} = 0,\ z = L \tag{10}$$

and initial condition:

$$\overline{T_p}(z,t) = 0,\ t = 0 \tag{11}$$

With:

$$\begin{aligned}\overline{\phi_p}\,(t) &= \frac{Q}{S}\left(-f_{exc} + \sum_{i=0}^{\infty}\delta\,(t - i\,P_{exc})\right)u\,(t)\\ &= \frac{Q}{S}\sum_{i=0}^{\infty}\delta\,(t - i\,P_{exc}) - f_{exc}\,[u\,(t - iP_{exc}) - u\,(t - (i+1)\,P_{exc})]\end{aligned} \tag{12}$$

The solution is:

$$\frac{\overline{T_p}\,(z,\,t)}{T_{lim}} = \sum_{i=0}^{\infty} y_\delta\left(\frac{z}{L},\,t - i\,P_{exc}\right) - f_{exc}\left[y_s\left(\frac{z}{L},\,t - i\,P_{exc}\right) - y_s\left(\frac{z}{L},\,t - (i+1)\;P_{exc}\right)\right] \tag{13}$$

Let $z^* = z/e$ a dimensionless position. $y_s\,(z^*,\,t)$ is the unit step response of the system:

$$y_s\,(z^*,\,t) = \left[t + 2\,g\,(z^*)\,\tau - 2\,\tau\sum_{k=1}^{\infty} a_k\,e^{-u_k^2\,t/\tau}\right]u\,(t)\,,\quad a_k = \frac{\cos\,(u_k\,z^*)}{u_k^2} \tag{14}$$

and $y_s\,(z^*,\,t)$ the unit impulse response:

$$y_\delta\,(z^*,\,t) = \left[1 + 2\sum_{k=1}^{\infty}\cos\,(u_k\,z^*)\;e^{-u_k^2\,t/\tau}\right]u\,(t) \tag{15}$$

Where $T_{lim} = Q/\rho C\,S\,L$ is the maximum possible peak-to-peak amplitude of $\theta\,(z^*,\,t^*)$, $\tau = L^2/a$ the conduction characteristic time, $u_k = k\,\pi$ and $g\,(z^*) = 1/6 - z^*/2\,(1 - z^*/2)$.

Strictly speaking, T_p is not periodic but becomes a P_{exc}-periodic function for large time. Let $\theta\,(z^*,\,t^*)$ be this function:

$$\begin{aligned}\frac{\theta\,(z^*,\,t^*)}{T_{lim}} &= 1 - \frac{2\,g\,(z^*)}{\alpha} - t^* +\\ &\qquad 2\sum_{k=1}^{\infty}\frac{\cos\,(u_k\,z^*)}{1 - \exp\,(-u_k^2\,\alpha)}\,e^{-u_k^2\,\alpha\,t^*},\;0 < t^* < 1\end{aligned} \tag{16}$$

With $t^* = t/P_{exc}$ a dimensionless time and $\alpha = P_{exc}/\tau$ the ratio between the thermal excitation repetition period and the characteristic conduction time. Figure 3 presents the

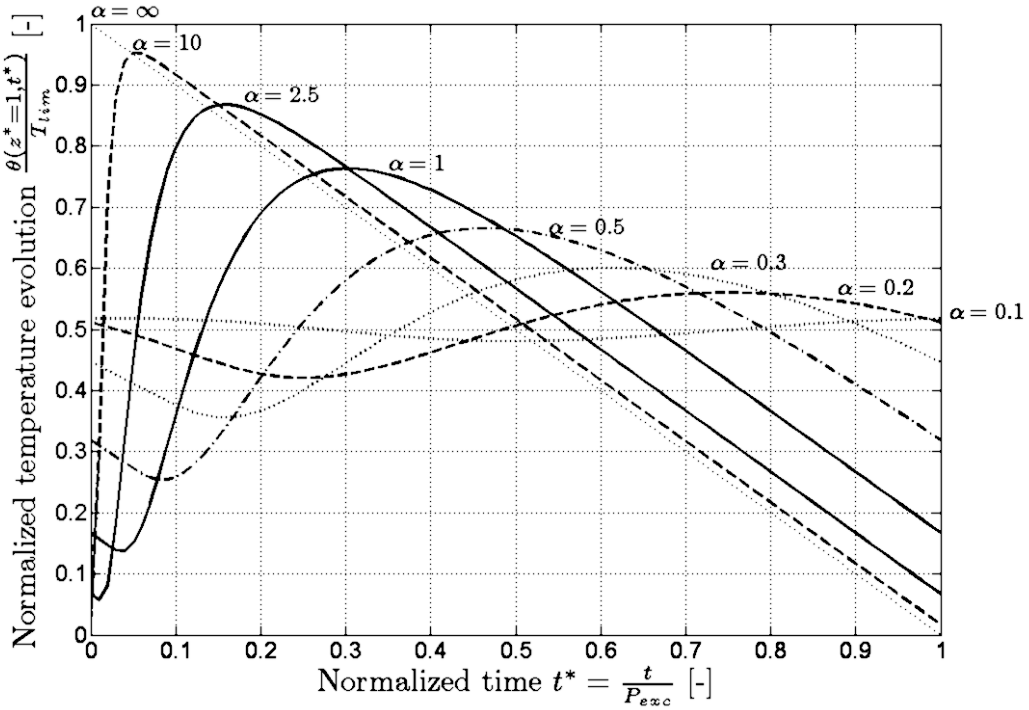

Figure 3: Normalized temperature evolution $\theta\left(z^*,\, t^*\right)/T_{lim}$ of the sample rear face ($z^* = 1$) according to α.

normalized temperature evolution of the sample rear face according to α. It is shown that a low α value leads to small temperature variations and the estimation of α will be compromised. On the opposite, if α is too high, the same conclusion holds since in that case, the temperature evolution carries hardly any information about α. Most of the curve is indeed independent of it. In practice, α is adjusted using the repetition frequency P_{exc} or the sample length L. The optimal value of α is discussed later.

It may be useful to increase the amount of energy absorbed by the sample since it would result in a higher T_{lim} value, i.e. a higher temperature variation. One way to do this consists in using a rectangular excitation of width Δt_{burst}. The corresponding solution $\theta_{burst}\left(z, t\right)$ can be retrieved either by a convolution product between 16 and the proper rectangular function, or by or replacing $y_\delta\left(z^*,\, t - i\, P_{exc}\right)$ by $1/\Delta t_{burst}\left[y_s\left(z^*,\, t - iP_{exc}\right) - y_s\left(z^*,\, t - iP_{exc} - \Delta t_{burst}\right)\right]$. It leads to:

$$\frac{\theta_{burst}\left(z^*,\, t^*\right)}{T_{lim}} = \frac{y_s\left(z^*,\, t\, P_{exc}\right) - y_s\left(z^*,\, \left(t^* - \lambda\right) P_{exc}\right)}{\Delta t_{burst}} - \frac{y_s\left(z^*,\, t\, P_{exc}\right)}{P_{exc}} + \frac{2}{\alpha\,\lambda} \sum_{k=1}^{\infty} \left[\frac{\left(1 - e^{-u_k^2 \alpha \lambda}\right)\left(e^{-u_k^2 \alpha (1-\lambda)}\right)}{\left(1 - e^{-u_k^2 \alpha}\right)} - \lambda \right] a_k\, e^{-u_k^2 \alpha (t^* - \lambda)}, \quad 0 \leq t^* \leq 1 \quad (17)$$

With $\lambda = \triangle t_{burst}/P_{exc}$ the dimensionless pulse width. For $t \leq \Delta t_{burst}$ and $t \geq \Delta t_{burst}$, relation 17 becomes respectively:

$$\frac{\theta_{burst}\left(z^*,\, t^*\right)}{T_{lim}} = \left(\frac{1-\lambda}{\lambda}\right)\left(t^* + \frac{2\,g\left(z^*\right)}{\alpha}\right) - \frac{2}{\alpha\,\lambda} \sum_{k=1}^{\infty} \frac{1 - e^{-u_k^2 \alpha (1-\lambda)}}{1 - e^{-u_k^2 \alpha}}\, a_k\, e^{-u_k^2 \alpha t^*}, \quad 0 \leq t^* \leq \lambda \quad (18)$$

$$\frac{\theta_{burst}\left(z^*,\, t^*\right)}{T_{lim}} = 1 - t^* - \frac{2\,g\left(z^*\right)}{\alpha} + \frac{2}{\alpha\,\lambda} \sum_{k=1}^{\infty} \frac{1 - e^{-u_k^2 \alpha \lambda}}{1 - e^{-u_k^2 \alpha}}\, a_k\, e^{-u_k^2 \alpha (t^* - \lambda)}, \quad \lambda \leq t^* \leq 1 \quad (19)$$

Figure 4 shows the evolution of the average temperature at the front and rear face of the sample with respect to α and λ. Increasing the pulse width λ tends to lower the amplitude of $\theta_{burst}(t^*)$. However, with most photothermal sources, increasing λ allows emitting more energy and this would compensate or at least limit the decrease of the absolute amplitude. Compared to the front face, the rear face temperature is higher at the end of each period ($t^* = 1$). This is due to the fact that temperature variations $\theta_{burst}(t^*)$ are relative to the steady temperature field $T_c\left(z^*\right)$.

Figure 5 presents the peak-to-peak amplitude of $\theta\left(z^*,\, t^*\right)$ and $\theta_{burst}\left(z^*,\, t^*\right)$ according to α and λ. Additionally, some key values of the amplitude are exhibited. It shows that the amplitude decreases as the repetition frequency f_{exc} increases. In addition, $\theta\left(z,\, t\right)/T_{lim} \to 1$ as $f_{exc} \to 0$. Obviously, f_{exc} can not be made arbitrarily low since it is related to the experiment duration and some experimental issues would arise. With a finite pulse duration, i.e. $\lambda > 0$, the maximum peak-to-peak amplitude of $\theta_{burst}\left(z,\, t\right)/T_{lim}$ is $1 - \lambda$ and is reached for $\alpha \to \infty$.

The heat transfer model has to be combined with the analog chain processing model

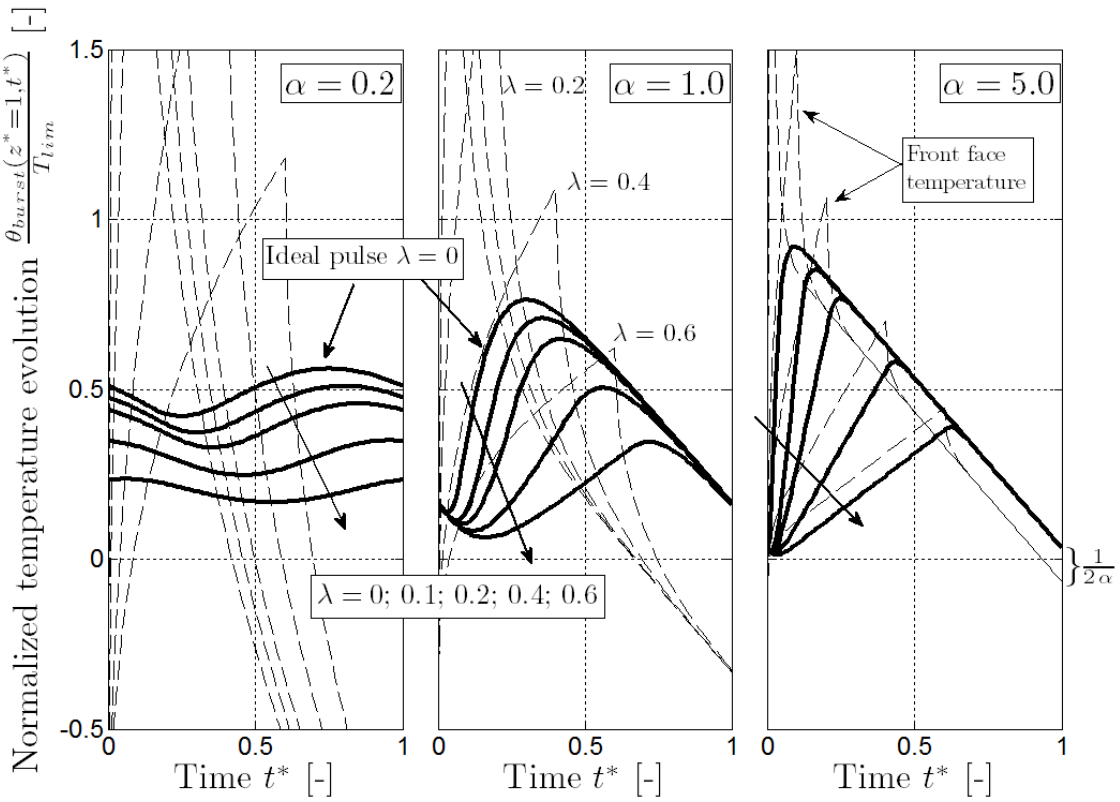

Figure 4: Temperature evolution at the front and rear face of the sample with respect to α and pulse width $\lambda = \Delta t_{burst}/P_{exc}$.

$H(j\,\omega)$. It could be done using a convolution product but it is more convenient to use Fourier series $\theta_{burst}(z^*, \omega_n)$ of temperature :

$$\theta_{burst}(z^*, t^*) = \sum_{n=-\infty}^{\infty} \theta_{burst}(z^*, \omega_n)\; e^{j\,\omega_n}, \quad \omega_n = 2\pi n \tag{20}$$

With:

$$\theta_{burst}(z^*, \omega) = \int_{t^*=0}^{1} \theta_{burst}(z^*, t^*)\; e^{-j\,\omega\,t^*} \mathrm{d}t^* \tag{21}$$

Using relations (18) and (19) with (21), it comes for $m > 0$:

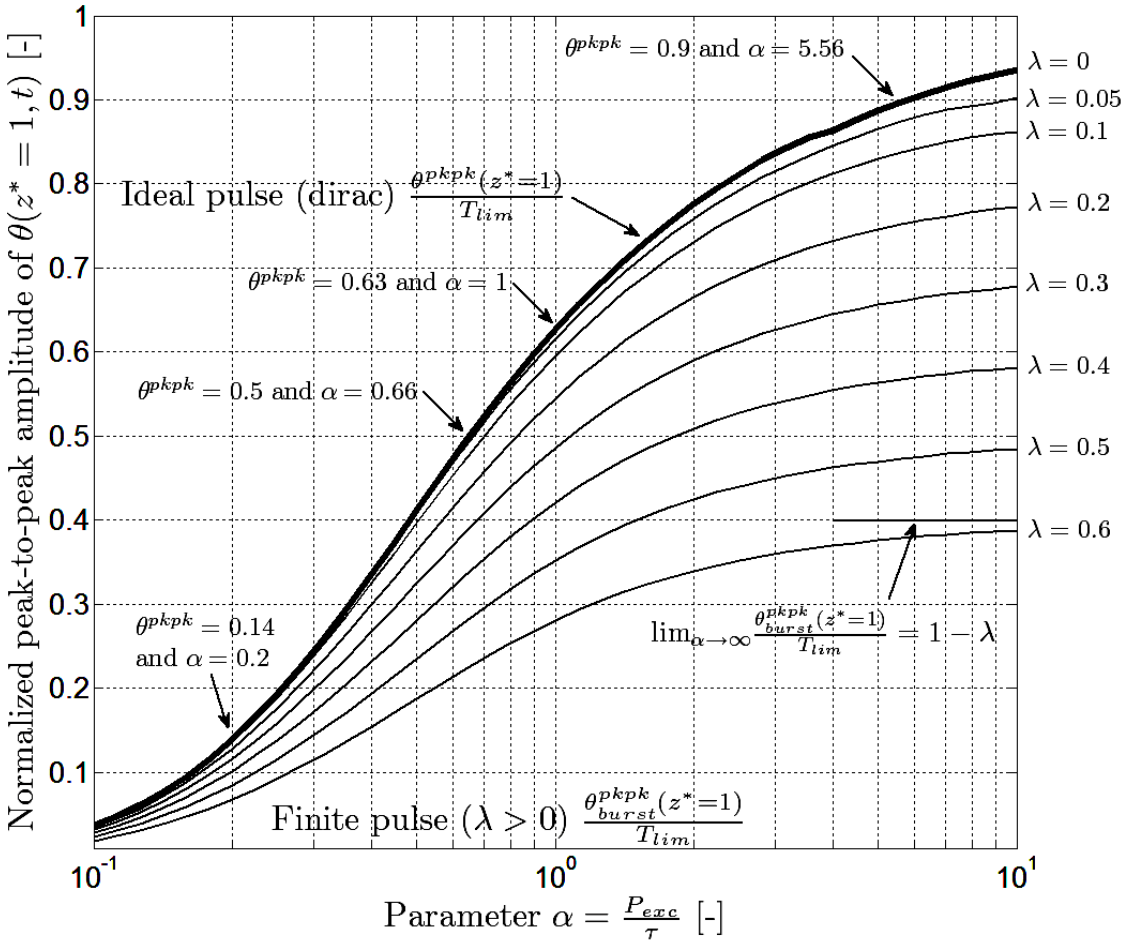

Figure 5: Peak-to-peak amplitude of normalized variations $\theta(z,\,t)/T_{lim}$ at the rear face ($z^* = 1$) with respect to α and pulse width $\lambda = \Delta t/P_{exc}$. The ideal dirac pulse is obtained for $\lambda = 0$.

$$\begin{aligned}\frac{\theta_{burst}(z^*,\,\omega)}{T_{lim}} = &-\frac{1-\lambda}{\lambda}\frac{1}{\alpha\omega^2}\left[\left(j2\omega g(z^*)+\alpha\right)\left(1-e^{-j\omega\lambda}\right)-j\alpha\lambda\omega e^{-j\omega\lambda}\right]\\ &-\frac{2}{\alpha\lambda}\sum_{k=1}^{\infty}a_k\frac{1-e^{-u_k^2\alpha(1-\lambda)}}{1-e^{-u_k^2\alpha}}\frac{1-e^{-\left(u_k^2\alpha+j\omega\right)\lambda}}{\alpha u_k^2+j\omega}\\ &-\frac{e^{-j\omega\lambda}}{\alpha\omega^2}\left[\left(j2\omega g(z^*)+\alpha\right)\left(e^{-j\omega(1-\lambda)}-1\right)+j\alpha\omega(1-\lambda)\right]\\ &-\frac{2}{\alpha\lambda}\sum_{k=1}^{\infty}a_k\frac{1-e^{-u_k^2\alpha\lambda}}{1-e^{-u_k^2\alpha}}\frac{e^{-u_k^2\alpha(1-\lambda)-j\omega}-e^{-j\omega\lambda}}{\alpha u_k^2+j\omega}\end{aligned} \tag{22}$$

For $m = 0$:

$$\frac{\theta_{burst}\left(z^*,\,\omega=0\right)}{T_{lim}} = \frac{\left(1-\lambda\right)\left(4g\left(z^*\right)+\alpha\lambda\right)}{2\alpha} - \frac{2}{\alpha^2\lambda}\sum_{k=1}^{\infty} a_k \frac{1-e^{-u_k^2\alpha(1-\lambda)}}{1-e^{-u_k^2\alpha}} \frac{1-e^{-u_k^2\alpha\lambda}}{u_k^2} + \frac{1-\lambda}{2\alpha}\left(\alpha\left(1-\lambda\right)-4g\left(z^*\right)\right) + \frac{2}{\alpha^2\lambda}\sum_{k=1}^{\infty} a_k \frac{1-e^{-u_k^2\alpha\lambda}}{1-e^{-u_k^2\alpha}} \frac{1-e^{-u_k^2\alpha(1-\lambda)}}{u_k^2} \tag{23}$$

Considering the transfer function of the filter/amplifier system derived in relation (1), the filtered temperature is finally:

$$\theta_{burst}^{filtered}\left(z^*,\,t^*\right) = \sum_{n=-\infty}^{\infty} \theta_{burst}\left(z^*,\omega_n\right)\, H_{f,n}\, e^{j\,\omega_n t^*} \tag{24}$$

With:

$$H_{f,n} = H\left(j\omega_n\right) = G\frac{-n^2\gamma^2}{1+j2m\gamma n-n^2\gamma^2}, \quad \gamma = \frac{f_{exc}}{f_c} \tag{25}$$

Evolution of $\theta_{burst}^{filtered}\left(z^*,\,t^*\right)/T_{lim}$ is shown in figure 6, considering different values of the filter parameters m and γ. To ease the comparison, the unfiltered temperature evolution has been shift down by the time-average temperature. The effect of the filter is barely visible for $f_{exc} > 100\, f_c$. In practice, such a filter is not always easy to design, especially if f_{exc} is low. Change the sample length could be a solution that would allow a higher repetition frequency to be used (γ would increase) while keeping α constant. Concerning the damping coefficient, the output signal appears to be quite insensitive as long as $m < 1$. Considering the repetition frequency f_{exc}, the cut-off frequency f_c, the characteristic conduction time τ, it is recommended to design the experiment in a way that $1/\tau \approx f_{exc} > 10\, f_c$.

IV. SENSITIVITY ANALYSIS AND EXPERIMENT OPTIMAL DESIGN

To deal with experimental considerations, the parameters C_0 is introduced in the equation (24).C_0 is the constant DC signal which is not necessarily zero due to various operational amplifier imperfections. Let $y\left(t\right)$ be the theoretical output signal:

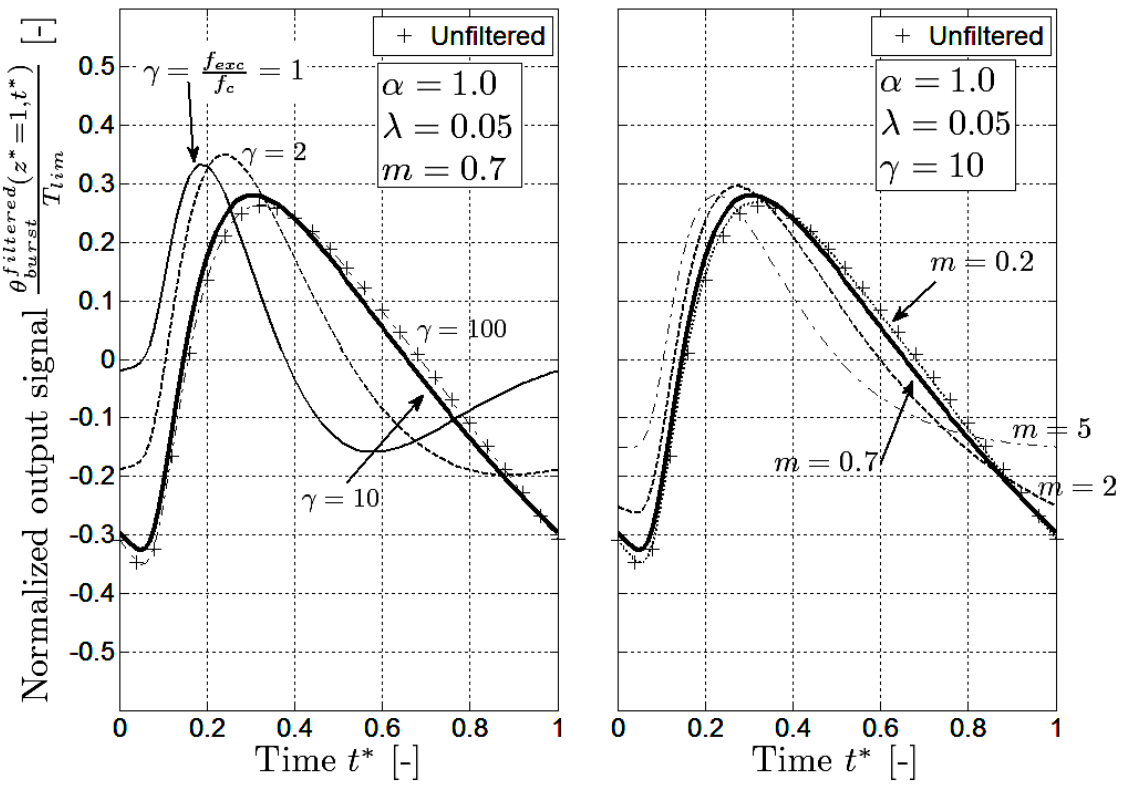

Figure 6: Evolution of $\theta_{burst}^{filtered}(z^*, t^*)/T_{lim}$ for different values of the filter parameters m and γ ($\alpha = 2.5$ and $\lambda = 0.05$ are fixed). The left plot shows the influence of the cut-off frequency f_c compared to the repetition frequency f_{exc}. The damping coefficient is fixed to $m = 0.7$. On the opposite, the right plot shows the influence of the damping coefficient. The cut-off frequency is fixed to $f_c = f_{exc}/10$.

$$y(t^*) = C_0 + y_{lim} \underbrace{\sum_{n=-\infty}^{\infty} \theta_{burst}(z^*, \omega_n)\, H_f(j\,\omega_n)\, e^{j\,\omega_n t^*}}_{f(\alpha,\gamma,m,t^*)}, \quad y_{lim} = G\,T_{lim} \tag{26}$$

Obviously the parameter to estimate is τ or $\alpha = P_{exc}/\tau$. In addition, y_{lim} and C_0 are also unknown and need to be estimated. Moreover, γ and m are only approximative and could be also affected by thermal drift, electronic component ageing or component non-linearity. Therefore, the vector of unknown parameters is $\mathbf{\Theta} = (\alpha, y_{lim}, C_0, \gamma, m)$. The sampling times are put in a vector $(t_1, \cdots, t_{Ndata})$. The sensitivity matrix X is then:

$$\mathbf{X} = \frac{\partial y}{\partial \Theta} = \underbrace{\begin{bmatrix} \frac{\partial f(-,t_1)}{\partial \alpha} & f(-,t_1) & 1 & \frac{\partial f(-,t_1)}{\partial \gamma} & \frac{\partial f(-,t_1)}{\partial m} \\ \vdots & \vdots & \vdots & \vdots & \vdots \\ \frac{\partial f(-,t_{ndata})}{\partial \alpha} & f(-,t_{Ndata}) & 1 & \frac{\partial f(-,t_{Ndata})}{\partial \gamma} & \frac{\partial f(-,t_{Ndata})}{\partial m} \end{bmatrix}}_{\mathbf{S}\,[\dim Ndata \times 6]} \underbrace{\begin{bmatrix} y_{lim} & & & & & \\ & 1 & & & & \\ & & 1 & & & \\ & & & y_{lim} & & \\ & & & & y_{lim} & \end{bmatrix}}_{\mathbf{D}\,[\dim 6 \times 6]} \tag{27}$$

To ease the following development, X is splitted in two matrices S and D. The benefit is that S does not depend on T_{lim} anymore. Simultaneous identification of all parameters Θ is possible if the associated sensitivity functions are linearly independent. Figure 7 presents the reduced sensitivity functions $X^* = X\,\mathrm{diag}(\Theta)$. Since C_0 is theoretically zero, corresponding reduced sensitivity was multiplied by 0.5 instead for plot purpose. For $\alpha = 1$ (middle plot) and $\alpha = 5$ (right plot), the maximum of $X^*(\alpha)$ is found at small times. As noted by Parker [1] with the flash method, the maximum sensitivity of α is close to the half-rise time of $\theta_{burst}(z^*, t^*)$ (see $X^*(y_{lim})$). In the left plot, this conclusion is still valid but maximum sensitivity of α is now near $t^* = 0.5$. These plots show a strong correlation between $X^*(\gamma)$and $X^*(m)$ which suggests that the amplifier/filter may be better identified separately with a specific experiment. Moreover, as α is made smaller, it is seen that all sensitivity amplitudes decrease. The reason is simply that the signal amplitude is reduced as shown by $X^*(y_{lim})$.

Let Y denotes experimental data. Without any regularization method and assuming the measurement noise is additive, Gaussian and iid with a standard deviation σ_m, the covariance matrix of Θ is given by $\mathbf{cov}(\Theta \mid Y) = \sigma_m^2\,\mathbf{D}^{-1}\left(\mathbf{S}^T\,\mathbf{S}\right)^{-1}\mathbf{D}^{-1}$. Therefore the standard deviation of α is given by:

$$\mathrm{std}(\alpha \mid Y) = \frac{\sigma_m}{y_{lim}} \sqrt{\left\{(S^T\,S)^{-1}\right\}_{1,1}} \tag{28}$$

Matrix dimension $S^T S$ increases with N_{data}. The influence of N_{data} on $\mathrm{std}(\alpha \mid Y)/\alpha$ is shown in Figure 8. Even if N_{data} is fixed, the first sample time sample has to be arbitrarily chosen. To avoid this, some jitter has been added to test all possible value of t_1^*, meaning that computations were done while shifting the whole time vector by a fraction of the time

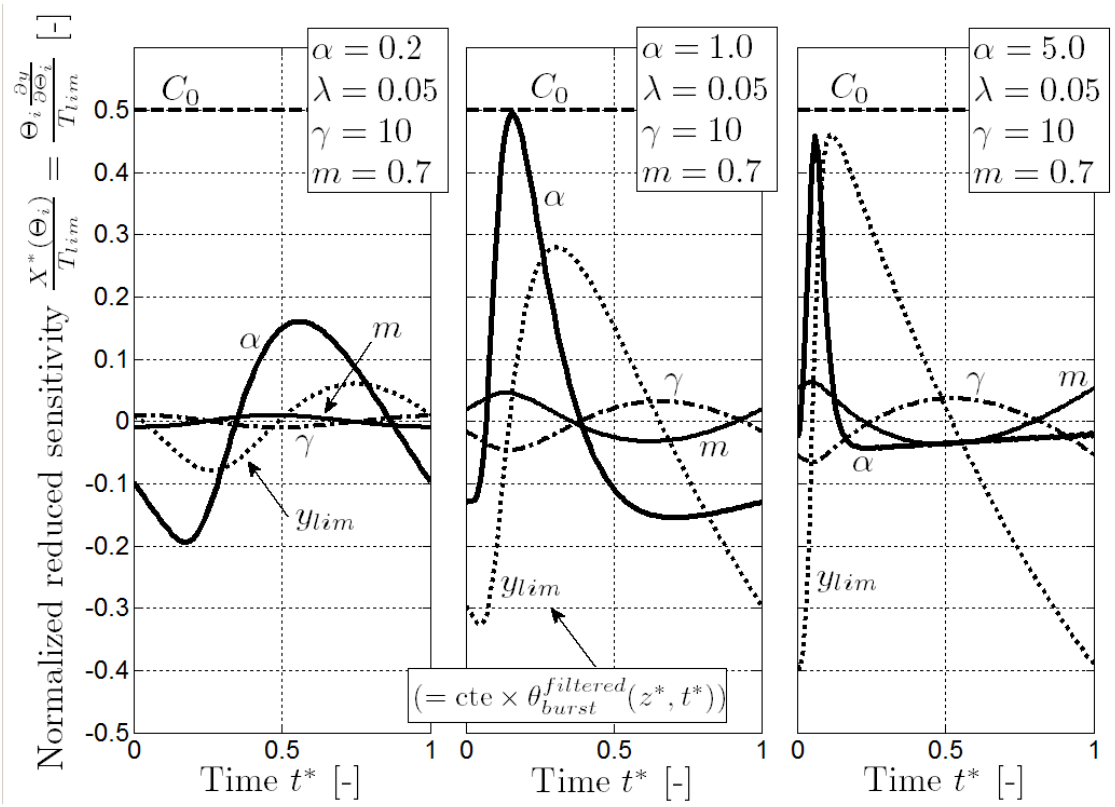

Figure 7: Reduced sensitivity functions $\Theta_i \frac{\partial y}{\partial \Theta_i}(z^*, t^*)$ normalized by T_{lim} with respect to t^*; $\alpha = \{0.2; 1; 2.5\}$ for left, middle and right plot respectively. Temperature evolution $\theta_{burst}^{filtered}$ is equal to $X^*(y_{lim})$ up to a constant factor.

step. The figure shows that above $N_{data} = 100$ or 200 samples/period the decreasing rate of $\text{std}(\alpha \mid Y)/\alpha$ in log-log scale is $1/2$. In other words, increasing the acquisition rate above these values only reduces the influence of measurement noise.

The objective is now to find the optimal experiment design, i.e. the theoretical values α and λ, that lead to the lowest standard deviation of α. Once found, the repetition period is then given for a specified sample by $P_{exc} = L^2\alpha/a$ and the pulse width $\Delta t_{burst} = \lambda P_{exc}$. In practice, the optimal design depends on thermal properties of the sample which are obviously unknown. Instead some reference values are used, that are likely to be closed to the real values.

From the point of view of the inverse problem (relation26), T_{lim} is an independent parameter. But from the experiment point of view, with most thermal source, like most lasers, T_{lim} depends on α and λ. Indeed, the output power is often fixed so that Q (and thenT_{lim}) depends linearly on Δt_{burst}. Let Φ be the photothermal output power absorbed by the sample. It comes from relation (28):

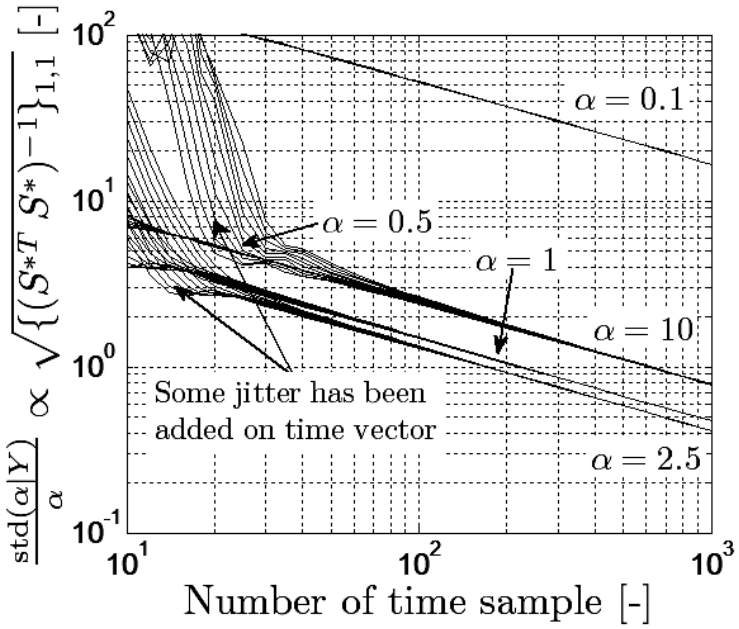

Figure 8: Normalized standard deviation of $\text{std}\,(\alpha \mid Y)\,/\alpha$ according to N_{data} and α.

$$T_{lim} = \frac{\Phi\lambda P_{exc}}{\rho C\, S\, L} = \frac{\Phi\lambda\alpha L}{S\, k} \quad \rightarrow \text{std}\,(\alpha \mid Y) = \frac{\sigma_m\, S\, k}{G\,\Phi L\,\alpha\lambda N_{data}^{1/2}} \sqrt{N_{data}\left\{(\mathbf{S}^T\, S)^{-1}\right\}_{1,1}} \tag{29}$$

The number of sample N_{data} has been explicitly introduced so that the term under the squareroot is nearly independent of N_{data}, at least for $N_{data} > 200$ as shown before. Using this relation, figure 9 (left plot) presents the relative standard deviation $\text{std}\,(\alpha \mid Y)\,/\alpha$ (up to the constant factor $\sigma_m S\, k/(G\,\Phi L\, N_{data}^{1/2})$) with respect to $0.1 \leq \alpha \leq 10$, $0.05 \leq \lambda \leq 0.9$ and for $N_{data} = 200$. This constant factor is omitted since it just appears as a constant coefficient and has no influence on the optimal point. It is seen that the effect of noise decreases as α is increased. The (local) minimum is obtained for $\alpha = 10.0$ and $\lambda = 0.5$. The corresponding standard deviation can be computed using the relation given in the figure. Compared to the traditional flash method which uses a short pulse width, the optimal excitation duration is found to be always $0.5\, P_{exc}$. Using a shorter excitation leads to a high dispersion of the estimations. For $\lambda = 0.1$ the standard deviation has increased by a factor of 1.5, for $\lambda = 0.05$, the factor is equal to 2.5. However contour lines show the tolerance is large. The minimum is indeed not very sensitive to α and γ. The optimal value of $\alpha = 10$ means that the repetition period P_{exc} should be 10 times the characteristic conduction time. But it could result in

a low repetition frequency f_{exc} meaning that the effect of the high-pass filter may become significant. In other words, uncertainties of f_c (and then γ) and m may generate large biases on the estimations. Let $\Omega = [\gamma;\, m]$ the supposedly-known parameters and $e_\Omega = [e_\gamma;\, e_m]$ the corresponding errors. Estimation biases can be approximated by a first-order development of the model around the solution of the identification problem [15]. The bias e_Θ generated is given by :

$$e_\Theta = -\left(X^T X\right) X^T X_\Omega e_\Omega \tag{30}$$

With X_Ω (dim $N_{data} \times 2$) the sensitivity matrix of parameters Ω. Parameters Ω can be seen as random variables and their uncertainty can be described by a Gaussian density distribution. The experiment turns out to be one realization of these two random variables. Thus, measurements are not only affected by noise but by random perturbations of γ and m as well. The covariance matrix of measurements is then $\mathbf{cov}\,(Y) = \sigma_m^2 I + X_\Omega \mathbf{cov}(e_\Omega)\, X_\Omega^T$. The covariance matrix of estimations is then :

$$\mathbf{cov}\,(\Theta \mid Y) = D^{-1}\left(S^T S\right)^{-1} S^T \mathbf{cov}\,(Y)\; S\left(S^T S\right)^{-1} D^{-1} \tag{31}$$

In particular, $\mathrm{std}\,(\alpha \mid Y)$ is:

$$\begin{aligned}\left(\mathrm{std}\,(\alpha \mid Y)\right)^2 = &\left(\frac{S\,k\,\sigma_m}{G\Phi L\, N_{data}^{1/2}}\right)^2 \frac{N_{data}}{(\alpha\lambda)^2}\left\{\left(S^T S\right)^{-1}\right\}_{1,1} \\ &+ \left(\frac{\sigma_\Omega}{\Omega}\right)^2 \left\{\left(S^T S\right)^{-1} S^T S_\Omega^* S_\Omega^{*T}\, S\left(S^T S\right)^{-1}\right\}_{1,1}\end{aligned} \tag{32}$$

With σ_Ω/Ω the relative standard deviation assumed equal for γ and m. The relation (32) depends on experimental parameters that can not be defined yet. But since they are just constant factors, the two parts of the relation can still be analyzed with respect to α,λ, γ and m (and possibly on the way sample times are distributed).

Whereas left plot shows the contribution of measurement noise only, i.e. σ_Ω is assumed to be zero in relation (32), the right plot assumes that $\sigma_m = 0$. The effect of supposedly known parameter Ω strongly increases as α is increased but is nearly independent of λ. Contrary to the noise effect, the design is improved by making α as low as possible. Moreover, once

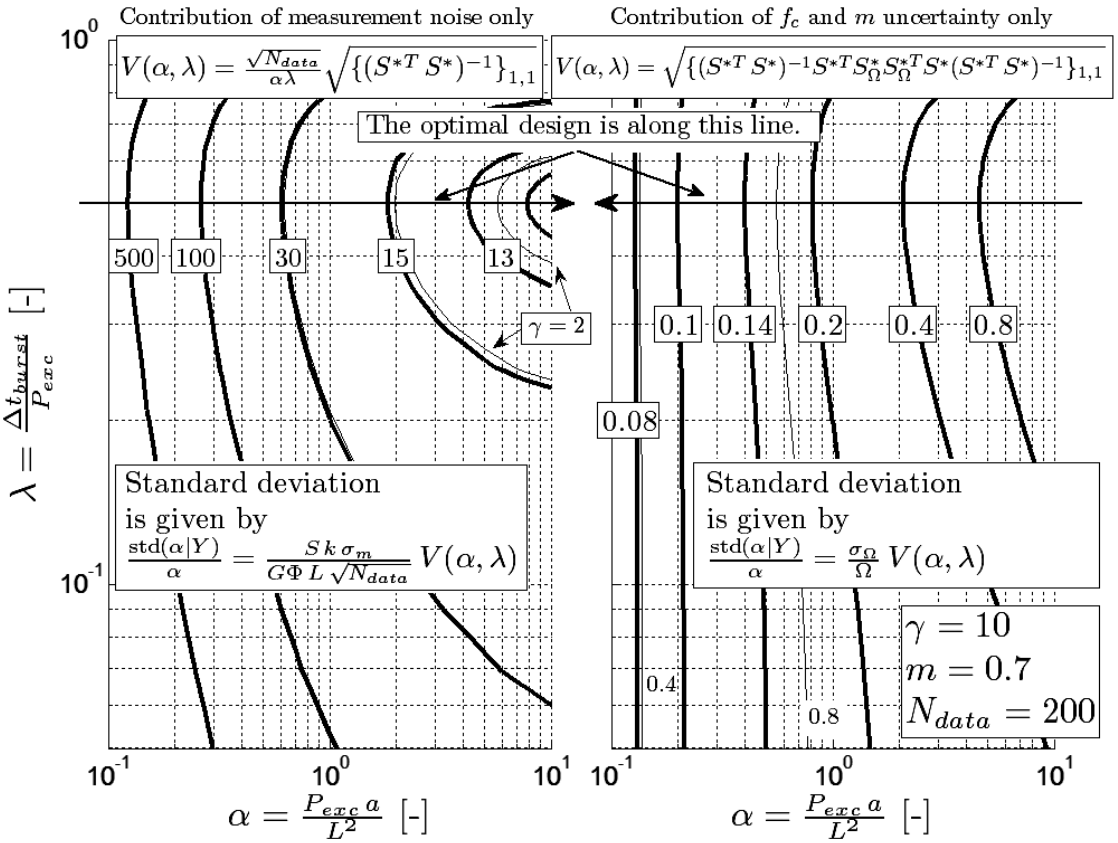

Figure 9: Contour graphs showing variations of the normalized standard deviation $\mathrm{std}(\alpha \mid y^*)/\alpha$ according to λ, α and $\gamma \in \{2; 10\}$. Thick lines refer to $\gamma = 10$ and thin lines to $\gamma = 2$.

α is fixed, the minimum influence of measurement noise is reached for $\lambda = 0.5$. On the contrary, it corresponds to the maximum influence of Ω. To compute $\mathrm{std}(\alpha \mid Y)$, these two plots has to be squared (variance) and summed with some coefficient (unknown at this stage). The resulting shape is not straighforward, but numerical analysis shows that whatever the experimental parameters are (in a raisonnable range), the optimal experiment design is reached for $\lambda = 0.5$. Compared to an ideal pulse, this 50% duty cycle emission leads to smoother temperature variations but the loss in sensitivity is compensate by a large increase of temperature variation, i.e. of the signal over noise ratio.

It is possible to go a step further by computing the optimal value $\hat{\alpha}$ with respect to the ratio between the two weighting coefficients of the relation 32. Let η be this ratio such that:

$$\left(\frac{\mathrm{std}\left(\alpha \mid Y\right)/\alpha}{\sigma_\Omega/\Omega}\right)^2 = \eta^2 \frac{N_{data}}{(\alpha\lambda)^2}\left\{\left(S^TS\right)^{-1}\right\}_{1,1} + \left\{\left(S^TS\right)^{-1} S^T S_\Omega^* S_\Omega^{*T} S \left(S^TS\right)^{-1}\right\}_{1,1}, \qquad \eta = \frac{S\,k\,\sigma_m}{G\Phi L\, N_{data}^{1/2}}\frac{\Omega}{\sigma_\Omega} \quad (33)$$

In practice, σ_Ω/Ω is roughly known, it is then possible to find the minimum of the left quantity according to η. A small value of η means that uncertainty of supposedly known parameter is dominant. On the contrary measurement noise is dominant if η is large. It leads to the figure 10. The duty cycle is fixed to the optimum value $\lambda = 0.5$ which has been numericaly checked for $10^{-4} \leq \eta \leq 10^{-1}$. It is seen that the optimal value $\hat{\alpha}$ (thick black line) is nearly proportionnal to η (in log-log scale). As a result, the relation between $\hat{\alpha}$ and η can be simplified using an power regression, such that $\hat{\alpha} \approx 7.5\,\eta^{0.45}$. To assess the sensitivity of this result to parameter γ, the corresponding optimal curve is shown in figure as well. The corresponding power regression is $\hat{\alpha} \approx 2.9\,\eta^{0.40}$.

Contour levels (left quantity of relation 33) show that the standard deviation of α slowly increases with η. It is therefore advisable to keep this parameter low. Dotted lines show that $\hat{\alpha}$ can be halved or doubled without significant negative effect on $\mathrm{std}\left(\alpha \mid Y\right)/\alpha$.

Figure 10 is useful to design an experiment. However, it's hardly possible to precisely evaluate the parameter η before the experiment is done. Instead, the experiment should be performed once with $\alpha = 1$ or any raisonnable value. The resulting estimations of α, y_{lim} and σ_m can be used to evaluate η with $\eta = \sigma_m \alpha \lambda y_{lim}^{-1} N_{data}^{-1/2} \left(\sigma_\Omega/\Omega\right)^{-1}$. The experiment is then performed again with a better value of α.

V. APPLICATION

In order to test previous results about the sensitivity study and the optimal experiment design, the method is applied on a sample made of copper ($L = 3.80 \pm 0.03$ mm) that has been elaborated in solid phase using the sintering process from Cu powder followed by an annealing at 950°C. Values of the specific heat per unit volume and the thermal conductivity of pure copper at ambient temperature (20°C) are well-known (see introduction). The expected values are $a = k/\rho\,C_p = 113\,\mathrm{mm^2.s^{-1}}$, $\tau = L^2/a = 0.128\,\mathrm{s}$. Front and rear surfaces of the sample have been polished roughly (average roughness is in the 10-20 µm range). The total

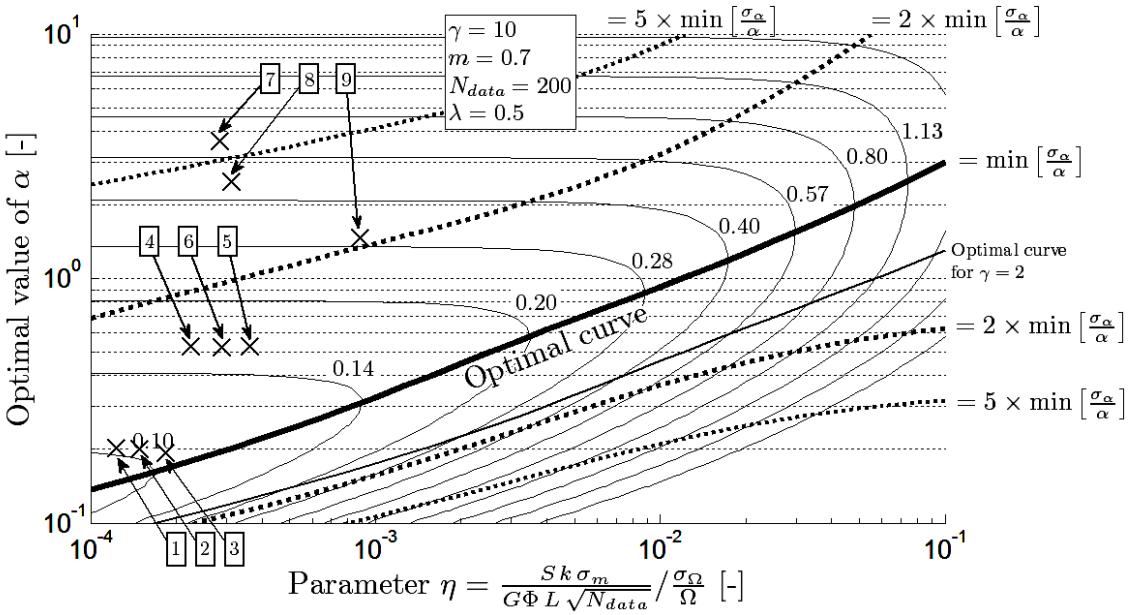

Figure 10: Optimal value of α according to η, for $\gamma = 10$ (thick black line) and for $\gamma = 2$ (black line). Dotted lines show the sensitivity of the minimum to α, i.e. boundaries corresponding to a multiplication by a factor of 2 (and 5) of the minimum standard deviation. Contour lines (thin black lines) refer to the left quantity of relation 33. Thus,$\mathrm{std}\left(\alpha \mid Y\right)/\alpha$ can be computed by multiplying the contour levels by σ_Ω/Ω. For information, the nine experiments performed and discussed in the last section are reported in this figure (crosses entitled 1 to 9).

hemispherical emissivity of the surfaces is less than 0.1. The internal laser frequency that control the pulse emission is set to $f_p = 90\,,\mathrm{kHz}$ and the number of pulses is adjusted to reach the desired value for Δt_{burst}. The number of sweeps is set to $N_s = 2000$ and the number of samples is around $N_{data} = 2000$.

The laser output power is about 10 W. The absorbed power Φ is then lower than 1 W. In the results shown below, the maximum absorbed energy lies in [52; 400] mJ. The corresponding values of T_{lim} are respectively [0.1; 1] K. The relative change in the detector resistance is computed to be about $\mathrm{d}R_{det}/R_{det} \sim 10^{-5}$ with $R_{det} \approx 100\,\Omega$. The peak-to-peak voltage across the detector resistor (filter/amplifier input) is of the order of magnitude of 10 to 100 μV. On the scope, the corresponding peak-to-peak voltage is lies in [3; 50] mV. The filter/amplifier gain is about 500, $f_c = 0.85\,\mathrm{Hz} \pm 10\%$ and $m = 0.70 \pm 10\%$.

Unknown parameters $\Theta = (\alpha,\, y_{lim},\, C_0)$ are identified from measurements Y by using a least squares estimator. The Levenberg-Marquardt algorithm [13] is used to solve the non-linear minimization problem. The corresponding objective function $J\left(\Theta\right)$ is:

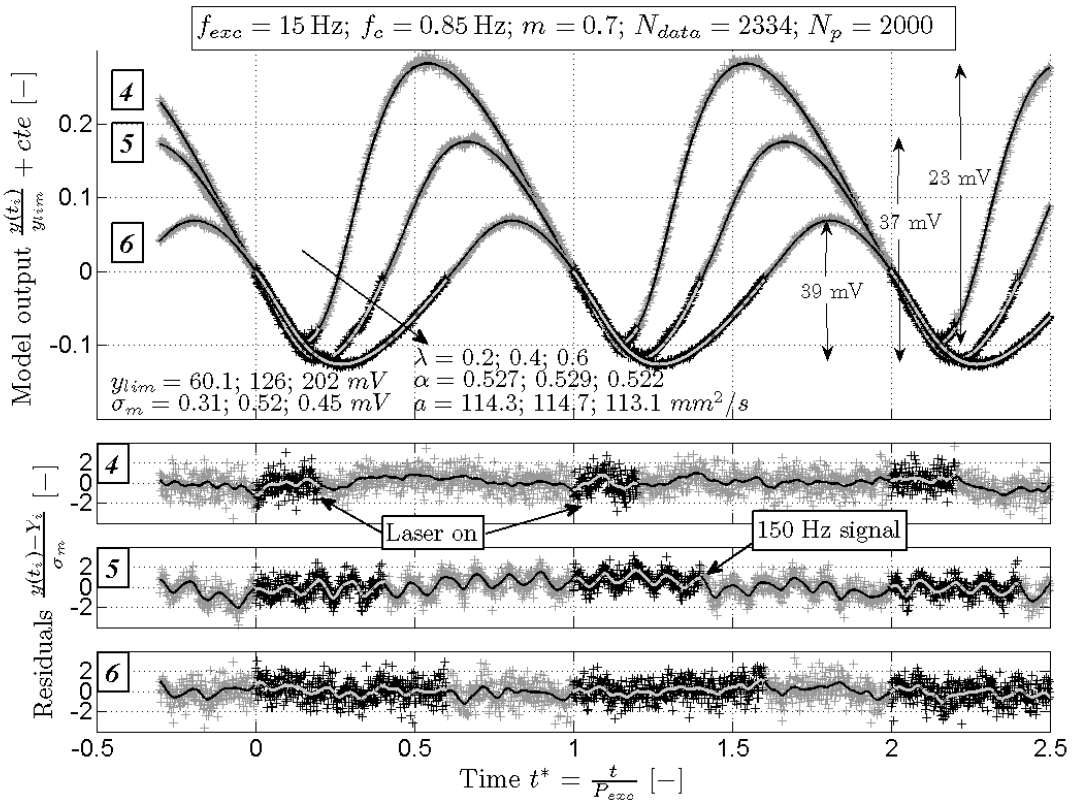

Figure 11: Configuration 4 to 6: Comparison between measurements Y and simulated data (model output) $y(t)$ for $f_{exc} = 15\,\mathrm{Hz}$ and $\alpha \approx 0.5$. Results are normalized by y_{lim} which depends on the configuration. The simulated data are represented in plain black lines whereas measurements are represented by gray crosses. To bring out potential biases, a moving average filter is applied on residuals (plain lines). Colors are inverted to highlight the laser on-state. Residuals are normalized by an estimation of the noise standard deviation.

$$J(\Theta) = \sum_{i=1}^{N_{data}} \left(y(\Theta, z^* = 1,\, t_i^*) - Y_i\right)^2 \tag{34}$$

Following the analysis in the previous section, standard deviations of the identified parameters are:

$$\sigma(\Theta) \approx \sqrt{\frac{J_{end}}{N_{data}}} \sqrt{\left\{(X^T X)^{-1}\right\}_{1,1}} \tag{35}$$

with J_{end} is the value of the objective function $J(\Theta)$ at the end of the minimization process.

Nine different configurations are tested with the same sample. α and λ were chosen in a large range to evaluate their influence. Results are shown in Table (II). Rows are sorted

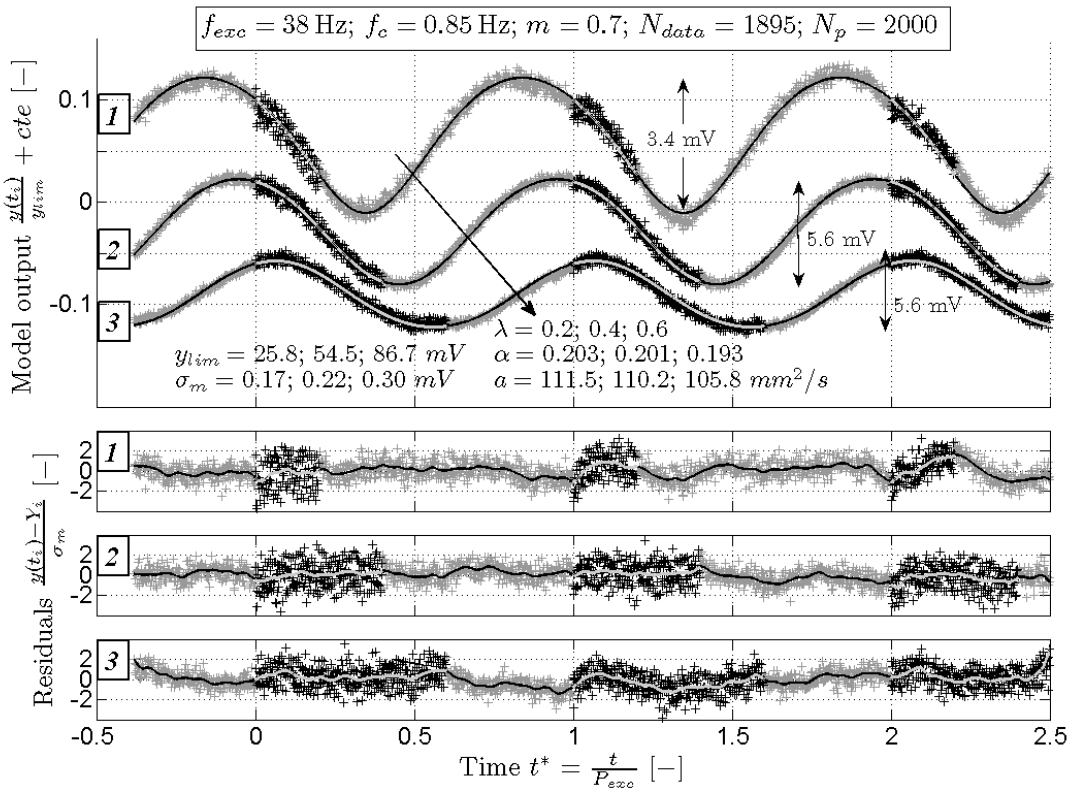

Figure 12: Configuration 1 to 3: Comparison between measurements Y and simulated data (model output) $y\,(t)$ for $f_{exc} = 38\,\mathrm{Hz}$ and $\alpha \approx 0.2$.

based on f_{exc}. Best results has given by configurations 4 to 6. The repetition frequency has been set to 15 Hz in such way that $\alpha \approx 0.5$ based on standard copper thermal properties. Whatever is the thermal excitation duration $\lambda = \{0.2;\ 0.4;\ 0.6\}$ the corresponding thermal diffusivity is closed to standard value. The 95%-confidence interval is ± 4 is mainly due to the uncertainty of L. Measurements and experimental data are reported in Figure 11. A 150 Hz signal is present with configuration 5 but it has no influence on the thermal diffusivity. About f_{exc} value, it should be chosen in a way that electrical grid perturbation are nullified by the average operation during the acquisition.

Configurations 1 to 3 aim at $\alpha = 0.2$. As predicted by the theory, Figure 12 shows that peak-peak amplitudes (around 5 mV) are much lower than in configuration 4 to 6 whose peak-peak amplitude is about 30 mV. Indeed, decreasing α from 0.5 to 0.2 reduces the product $\alpha\lambda$ and them T_{lim} by a factor 2.5. Additionaly, relative amplitude decreases simultaneously to α. Figure 5 shows that the peak-peak amplitude is reduced by a factor 3. As a result, measurements are more sensitive to perturbations coming from the electrical

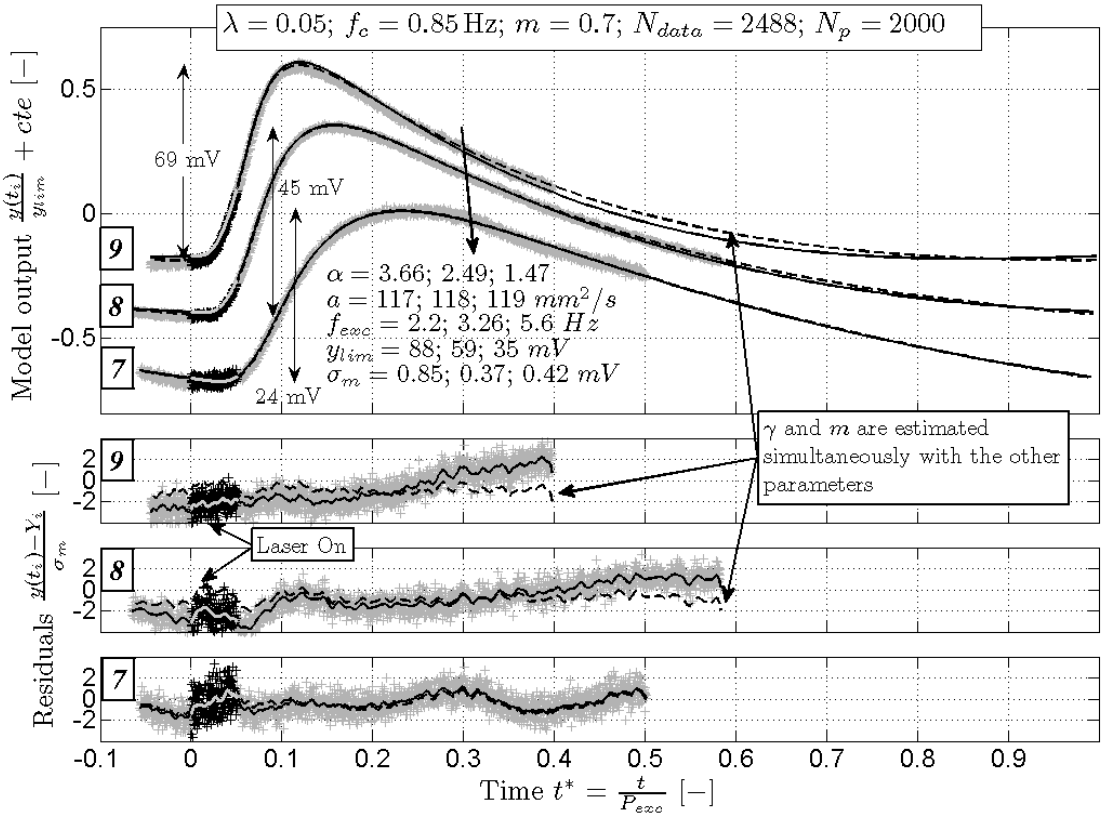

Figure 13: Configuration 7 to 9: Comparison between measurements Y and simulated data (model output) $y(t)$ for $\lambda = 0.05$ and $f_{exc} = \{2.2; 3.26; 5.6\}$ Hz.

grid, the laser state switch, the scope trigger... A correlation between the laser state and the residual dispersion is visible in configuration 1 to 3.

Concerning columns 7 and 8, as suggested by the previous analysis, increasing α from 0.2 to 0.5 halves the noise influence but increase the sensitivity to supposedly known parameters Ω by a factor 5. As shown in figure 10, configuration 1 to 3 are closer the optimal design which lead to lower theoretical standard deviations of α (as shown in column 3). Strictly speaking, this figure is only given for the optimal duty cycle $\lambda = 0.5$, but the information it gives should still be relevant for $\lambda = 0.4$ or $\lambda = 0.6$.

Configuration 7 to 9 are slightly different (Figure 13). The acquisition window is concentrated on one pulse only and particularly on small times. Some numerical tests has been carried out and it appears this practice does not lead to better results. As the window is made smaller to increase the number of measurements during the temperature rise, standard deviation of α is getting worse due to a increasing sensitivity to the noise. However, it may be a way to select time samples insensitive (or less sensitive) to filter parameters. Thermal diffu-

N°	$f_{exc}\,Hz$	$\alpha\left(\pm 2\,\frac{\sigma_\alpha}{\alpha}\right)^{(a)}$	λ	γ	$a\,(\pm 2\sigma_a)^{(b)}\,\frac{mm^2}{s}$	$\sigma_m \to 2\sigma_a/a$	$\sigma_\Omega \to 2\sigma_a/a$
1	38	0.203 (0.4%)	0.2	45	112 ± 5	$15\%/\sqrt{N_{data}}$	0.2%
2	38	0.201 (0.4%)	0.4	45	110 ± 4	$11\%/\sqrt{N_{data}}$	0.2%
3	38	0.193 (0.4%)	0.6	45	106 ± 4	$15\%/\sqrt{N_{data}}$	0.2%
4	15	0.528 (1%)	0.2	18	$\underline{114 \pm 4}$	$6\%/\sqrt{N_{data}}$	1%
5	15	0.530 (1%)	0.4	18	$\underline{115 \pm 4}$	$6\%/\sqrt{N_{data}}$	1%
6	15	0.522 (1%)	0.6	18	$\underline{113 \pm 4}$	$5\%/\sqrt{N_{data}}$	1%
7	5.6	1.47 (3%)	0.05	6.7	119 ± 5	$11\%/\sqrt{N_{data}}$	3%
	$5.6^{(c)}$	1.46 (0.5%)	0.05	16 (10%)	118 ± 4	$24\%/\sqrt{N_{data}}$	-
8	3.26	2.50 (6%)	0.05	3.8	118 ± 8	$7\%/\sqrt{N_{data}}$	6%
	$3.26^{(c)}$	2.50 (0.2%)	0.05	7.1 (2%)	118 ± 4	$11\%/\sqrt{N_{data}}$	-
9	2.2	3.7 (9%)	0.05	2.6	117 ± 11	$11\%/\sqrt{N_{data}}$	9%
	$2.2^{(c)}$	3.8 (0.3%)	0.05	3.2 (2%)	121 ± 4	$16\%/\sqrt{N_{data}}$	-

(a) Uncertainty of α is computed using relation (32). The 95%-confidence intervals are: $f_c \pm 10\%$; $m \pm 10\%$.

(b) Uncertainty of a is given by: $(\sigma_a/a)^2 = (\sigma_\alpha/\alpha)^2 + 4\,(\sigma_L/L)^2$.

(c) f_c and m are considered unknown and are estimated simultaneously to other parameters. Estimation dispersion is now only due to measurement noise.

Table II: Identification of a according to f_{exc} and $\lambda = \Delta t_{burst}/P_{exc}$. The estimation of α in each configuration is presented in column 3. The corresponding thermal diffusivity is given in column 6 by $a = \alpha L^2 f_{exc}$ with $L = 3.8\,\text{mm} \pm 0.06$. Column 7 and 8 show the effect of measurement noise and supposedly known parameter uncertainty on the estimated diffusivity. They contain the confidence interval that would occur if $\sigma_\Omega = 0$ and $\sigma_m = 0$ respectively.

sivities estimated with these configurations are slightly overestimated but are nearly constant which suggests an bias issue resulting from errors of Ω or from model inadequacy. If γ and m are not fixed anymore but are estimated, the two additional degree of freedom improve the fit quality significantly, but the corresponding estimated cutoff frequency and damping coefficient are not coherent: $(0.35 \pm 10\%;\ m = 1.8 \pm 10\%)$, $(0.45 \pm 2\%;\ m = 1.32 \pm 2\%)$, $(0.69 \pm 2\%;\ m = 0.83 \pm 3\%)$ for configuration 7, 8 and 9 respectively. Moreover, a second effect of estimating these parameters is a large decrease of the standard deviation of α but it's purely theoretical. This precision is overestimated.

VI. CONCLUSION

The method presented in this paper is an improvement of the well-known flash method. The objective is to deal with highly diffusive materials with low optical emission/absorption

coefficient. Instead of increasing this optical coefficient using coating, this approach is based on a noise reduction technique that allows increasing greatly the signal over noise ratio. It consists in heating a sample periodically with a photothermal excitation at the front face while recording the rear face temperature after every heat sequence. Contrary to the standard flash method which relies on just one flash, the proposed method makes use of hundreds or even thousands flash. Since the measurement noise is generally statistically independent, averaving all these sequences reduces the noise standard deviation.

This work shows the benefit of a sample-dependent electronic processing. Indeed, caution has been put on the analog signal processing to make the best use of the acquisition device. Thanks to a high-pass filter, measurements are recorded with the highest sensitivity without degrading the transient evolution of the signal. An identification procedure of the thermal diffusivity and the analog filter parameters has been implemented. This approach uses a complete analytical model of heat transfer and analog processing.

A sensitivity analysis has been performed in order to optimize the experiment design, i.e. the repetition frequency and the photothermal source duty cycle. It was shown that the ideal dirac pulse is not optimum with this technique. Instead a 50% duty cycle should be use to minimize theoretical uncertainty computed by taking into account measurement noise and uncertainty on some supposedly known parameters. Additionally, longer pulse width is convenient with most photothermal sources since it allows more energy to be emitted.

An application is presented on a sample made of sintered copper. It shows the reliability of the proposed method. The results are in good agreement with the theoretical expectations.

Acknowledgments

This study has been done thanks to the FUI MC+ project funded by the BPI (Banque Publique d'Investissement, France).

---

[1] W. J. Parker, R. J. Jenkins, C. P. Butler, G. L. Abbott, Flash method of determining thermal diffusivity, heat capacity, and thermal conductivity, J. Appl. Phys. 32 (1961) 1679-1684.

[2] T. Baba, M. Kobayashi, A. Ono, J. H. Hong, M. M. Suliyanti, Experimental investigation of the nonuniform heating effect in laser flash thermal diffusivity measurements, Thermochim.

Acta 218 (1993) 329-339.

[3] A. Degiovanni, G. Sinicki, M. Laurent, Heat Pulse Thermal Diffusivity Measurements-Thermal Properties Temperature Dependence and Non-Uniformity of the Pulse Heating, in Thermal Conductivity 18 (1985) (New York: Plenum) p. 537.

[4] D. Maillet, S. André, A. Degiovanni, Les erreurs sur la diffusivité thermique mesurée par méthode flash : confrontation théorie-expérience [in French] J. Phys. III 3 (1993) 883-909 [https://hal.archives-ouvertes.fr/jpa-00248966].

[5] T. Baba, A. Ono, Improvement of the laser flash method to reduce uncertainty in thermal diffusivity measurements, Meas. Sci. Technol. 12 (2001) 2046-2057.

[6] L. Vozär, W. Hohenauer, Flash method of measuring the thermal diffusivity. A review, High Temperatures-High Pressures 35/36 (2003/2004) pages 253-264.

[7] F. Cernuschi, L. Lorenzoni, P. Bianchi, A. Figari, The effects of sample surface treatments on laser flash thermal diffusivity measurements, Infrared Physics & Technology 43 (2002) 133–138.

[8] Seog-Kwang Kim, Yong-Jin Kim, Determination of apparent thickness of graphite coating in flash method, Thermochimica Acta 468 (2008) 6–9.

[9] Kuk-Hee Lim, Seog-Kwang Kim, Myung-Kyoon Chung, Improvement of the thermal diffusivity measurement of thin samples by the flash method, Thermochimica Acta 494 (2009) 71–79.

[10] D. Maillet, C. Moyne, B. Rémy, Effect of a thin layer on the measurement of the thermal diffusivity of a material by a flash method, International Journal of Heat and Mass Transfer 43 (2000) 4057–4060.

[11] L. Vozár, G. Labudová, and W. Hohenauer, The Laser Flash Method with Repeated Pulses—Optimal Experimental Design Analysis, International Journal of Thermophysics 23(5) (2002) 1157–1170.

[12] A. B. Williams, Analog filter and Circuit design handbook, Mc Graw-Hill 2006.

[13] J. V. Beck and K. J. Arnold, Parameters estimation in engineering and science, Dept. of Statistics and Probability, Michigan State University; Revised edition (1976).

[14] Handbook of condensed matter and materials data, W. Martienssen and H. Warlimont (Eds.), Springer Berlin Heidelberg New York 2005.

[15] E. Ruffio, D. Saury, D. Petit, Robust experiment design for the estimation of thermophysical parameters using stochastic algorithms, International Journal of Heat and Mass Transfer 55 (2012) 2901-2915